Safavi-Sohi *et al. Cell Communication and Signaling* (2025) 23:308
https://doi.org/10.1186/s12964-025-02273-1

Cell Communication and Signaling

RESEARCH Open Access

Peritoneal cavity-derived small extracellular vesicles from aged tumor-naïve hosts promote ovarian cancer adhesion and invasion

Reihaneh Safavi-Sohi[1†], Jeff Johnson[2,3†], Yueying Liu[2,3], Jing Yang[2,3], Tyvette S. Hilliard[4], Zhikun Wang[2,3], Christopher Barile[2], Josh Mijares[2], Ceming Wang[5,6], Hsueh-Chia Chang[3,5], Rebecca J. Whelan[7†] and M. Sharon Stack[2,3*†]

Abstract

Background Epithelial ovarian cancer (OvCa) remains a leading cause of mortality among gynecological cancers. Metastasis to the peritoneum, characterized by tumor cell adhesion to and invasion of the mesothelial lining of the abdominal cavity, represents a critical early event in OvCa metastatic progression. The median age of diagnosis is 63 and there exists a strong correlation between advanced age, OvCa incidence and disease stage. Moreover, the aged peritoneal cavity represents a permissive niche for metastatic dissemination.

Methods To investigate age-related factors that influence host-tumor communication in metastatic progression, the current study isolated small extracellular vesicles (sEVs) from the peritoneal lavage of healthy tumor-naïve young (3–6 month) and aged (20–22 month) mice. sEVs were analyzed using LC-MS/MS to identify sEV protein cargoes and incubated with murine and human OvCa cells to evaluate effect on pro-metastatic behaviors.

Results Treatment of human or murine OvCa cells with sEVs from healthy aged hosts significantly enhanced adhesion to peritoneal mesothelial cells in a three-dimensional in vitro meso-mimetic culture assay and to the intact omentum in a short-term in vivo adhesion assay relative to OvCa cells treated with sEVs from young hosts. OvCa cell invasion of collagen gels was also enhanced by aged host-derived sEVs. Proteomic analysis of sEV protein cargos identified differentially expressed proteins in sEVs obtained from aged vs. young hosts that may play a significant role in regulation of adhesion. This was confirmed using meso-mimetic adhesion assays with function blocking antibodies or small molecule inhibitors, supporting a potential role for several proteins in promoting intra-peritoneal dissemination in the aged host.

†Reihaneh Safavi-Sohi and Jeff Johnson contributed equally to this work.

†Rebecca J. Whelan and M. Sharon Stack are co-senior authors.

*Correspondence:
M. Sharon Stack
sstack@nd.edu

Full list of author information is available at the end of the article

Conclusions Results suggest that sEVs derived from the aged peritoneal microenvironment can contribute significantly to disease progression, highlighting sEV-mediated host: tumor communication as a potential therapeutic target for intervention in OvCa progression or recurrence in the aged host.

Keywords Extracellular vesicle, Ovarian cancer, Aging, Adhesion, Invasion, Metastasis, Proteomics, Mesothelium

Introduction

With nearly 20,000 new cases and 13,000 deaths annually in the United States, ovarian cancer (OvCa) is the most fatal disease of gynecologic origin [1, 2]. While the overall 5-year survival rate is 50%, the majority of patients are diagnosed with late-stage disease with a survival rate of 31% [1–3]. The high mortality rate among women with OvCa is directly attributable to widespread intra-peritoneal (i.p.) metastasis, indicating that elucidating factors that regulate metastasis can translate into clinical strategies to limit i.p. dissemination of primary and recurrent tumors. Metastasis results from exfoliation of tumor cells into the peritoneal cavity with initial homing to the omentum [3, 4]. From the omentum, tumors spread throughout the abdominal peritoneum generating widely disseminated i.p. carcinomatosis [3]. Both the omentum and the remainder of the abdominal peritoneum are overlaid by a monolayer of peritoneal mesothelial cells that represent the initial sites of host: tumor interaction in metastasis. Following adhesion, disseminating OvCa cells induce mesothelial cell retraction and exposure of the underlying three-dimensional collagen-rich sub-mesothelial matrix, into which cells migrate, anchor and proliferate to generate widely disseminated secondary lesions [3, 4]. Accumulation of peritoneal ascites fluid occurs in more than 80% of metastatic cases, frequently in high volumes, and provides an additional vehicle for i.p. tumor cell dissemination as well as a depot of cellular and soluble factors that influence tumor cell survival and behavior.

The median age of OVCA diagnosis is 63 and there exists a strong correlation between advanced age, tumorigenesis and disease stage [2, 5]. In addition to increased incidence with age, elderly patients have poor progression-free and overall survival relative to younger women [6–10]. Using two distinct pre-clinical models of OvCa, we have previously demonstrated that aged mice develop consistently greater overall tumor burden, omental and peritoneal metastases, and malignant ascites relative to young mice [11, 12]. These studies also highlighted age-related changes in omental ultrastructure that establish a permissive metastatic niche for OvCa metastatic dissemination to the aged omentum. To further evaluate host: tumor communication in metastatic progression, the current study examines small extracellular vesicles (sEVs) present in peritoneal lavage fluid obtained from tumor-naïve aged vs. young hosts. sEVs are intimately involved in intercellular communication by transporting biologically active molecules between cells and have been shown to influence tumor progression by modulating angiogenesis, epithelial-mesenchymal transition, cell adhesion, migration, invasion, matrix remodeling, inflammation and immune evasion [13–19]. Our results show that sEVs obtained from healthy aged hosts promoted tumor cell: mesothelial cell interaction in vitro and in vivo and enhanced tumor cell invasive behavior through three-dimensional collagen gels. The protein content of sEV from young and aged hosts was analyzed by comparative high-throughput nano-liquid chromatography-MS/MS (LC-MS/MS) technology with label-free quantification of total ion currents collected from the MS data. Results show unique sets of proteins in sEVs obtained from aged vs. young hosts that reveal changes in the peritoneal microenvironment with aging and thus may play a significant role in regulation of metastatic progression in the aged host.

Materials and methods

General reagents

Unless otherwise stated, all solvents (Ultra LC – MS grade) were purchased from J.T.Baker (VWR). Acetic acid (AA), sodium dodecyl sulfate (SDS), iodoacetamide (IAA), andtriethylammonium bicarbonate (TEAB) were purchased from Millipore Sigma (St. Louis, MO). Tris(2-carboxyethyl)phosphine (TCEP), deoxycholic acid (DCA), phosphoric acid, methanol, 0.1% formic acid (FA) in water, and sodium hydroxide (NaOH) were obtained through VWR. Pure FA (99% purity), acetonitrile (ACN), and Polystyrene-divinylbenzene (SDB-RPS) StageTips™ were purchased from Fisher Scientific (Hanover Park, IL). Trypsin/Lys-C Mix (Mass Spec Grade) was purchased from Promega (Madison, WI), and S-Traps™ were purchased from Protifi (Huntington, NY). The NanoOrange™ Protein Quantitation Kit was purchased from Thermo Fisher (Waltham, MA).

Cell culture

The human OvCa cell lines OVCAR5 and OVCAR8 were maintained in Dulbecco's Modified Eagle Medium (DMEM, Corning Cellgro) with 10% fetal bovine serum (FBS; Gibco), 1% nonessential amino acids (Corning Cellgro), and 1% penicillin/streptomycin (Corning Cellgro). The human peritoneal mesothelial cell line LP9 cell line was obtained from Coriell Institute for Medical Research (#AG07086, Camden, NJ) and maintained in a 1:1 ratio of M199 and Ham F12 media (Gibco), supplemented

with 15% FBS, 1% penicillin/streptomycin, 1% HEPES (Corning Cellgro), 1% GlutaMAX (Gibco), 10 ng/ml of epidermal growth factor (Sigma), and 400 ng/ml of hydrocortisone (Sigma). The murine C57Bl/6 syngeneic ovarian cancer cell line ID8-Trp53$^{-/-}$was generously provided by Dr. McNeish [20], and tagged with red fluorescent protein (RFP) as previously described [21]. Cells were maintained in DMEM containing 4% FBS, 1% Penicillin/Streptomycin, and supplemented by 5 µg/mL Insulin, 5 µg/mL Transferrin, and 5 ng/mL Sodium Selenite (1% ITS; Sigma).

Murine peritoneal lavage

Female C57/Bl6 mice were obtained from Jackson Laboratories (Bar Harbor, ME) with approval of the University of Notre Dame Institutional Animal Care and Use Committee. PBS (6 ml) was injected into the peritoneal cavities of young (3–6 month, equivalent to 20–30 y.o. human) or aged (22–24 month old, equivalent to 60–67 y.o. human) [22] tumor naïve C57Bl/6 mice using a syringe with an 18-gauge needle. After gently rocking the mouse several times, liquid peritoneal contents were removed using a syringe with a 24-gauge needle and kept on ice. Lavages were centrifuged for 10 min at 2000 g at 4 °C, and the supernatant was collected and stored at -80 °C or used immediately for EV isolation.

Small EV isolation

Peritoneal lavage supernatants were centrifuged at 10,000 g for 10 min at 4 °C and then were filtered through a 0.2 µm PES syringe filter. Typical sample size was 5 ml. sEVs were isolated using the NanoEX™ system, a bionanoparticle isolation technology (Aopia Biosciences, Pleasanton, CA), utilizing a microfluidic sEV isolation cassette according to manufacturer's specifications. sEVs were isolated from the lavage fluids of 5 young and 5 aged mice.

NanoSight nanoparticle tracking analysis (NTA)

sEV sizes and concentrations were determined using the NanoSight nanoparticle tracking analysis (NTA) instrument (NS300, Software Version: NTA 3.2 Dev Build 3.2.16; Malvern Panalytical, Malvern WR14 1XZ, UK). Immediately following sEV isolation, 1 ml of a diluted sample (typically 1:10 to 1:100) was introduced to the Low Volume Flow Cell by the NS300 Syringe Pump at a flow rate of 1000 (arbitrary software units) until particles were seen and about 0.1 ml of sample had been used. The syringe pump speed was gradually reduced to 50 and 60 s readings ($n = 5$) were captured at settings Gain 8 and Camera Level 10. Data were evaluated by Student's t-test using Sigmaplot version 15.0 with a p-value cutoff of 0.05 defined as statistically significant.

Transmission electron microscopy

sEVs were fixed in 2% Paraformaldehyde in PBS for 20 min. Formvar/Carbon 200 mesh Copper Grids (EMS #FCF200-CU-50) were washed twice in ddH_2O, and air-dried for 10 min. Grids were then inverted onto a 10 µl drop of UranyLess (EMS #22409) for 40–60 s., blotted off, and air-dried for 10 min. and stored dry at RT. Imaging was performed on a JEOL 2011 or a Talos F200i field emission transmission electron microscope. Four images were evaluated per age group with a minimum of 10 sEVs measured per image. Data were evaluated using the Mann-Whitney Rank Sum test using Sigmaplot version 15.0.

Western blot

EVs were incubated with ice-cold modified radio-immunoprecipitation assay (mRIPA) lysis buffer (50 mmol/l Tris pH 7.5, 150 mmol/l NaCl, 0.1% SDS, 1% Triton X-100, 5 mmol/l EDTA) for one hour on ice. For confirmation of EV marker proteins, lysates (20 µg) were electrophoresed on 9% SDS-polyacrylamide (SDS-PAGE) gels. For validation of proteomics data, lysates from 6×10^7 exosomes were loaded into each lane and electrophoresed on 9% SDS-PAGE gels. Gels were transferred to a polyvinylidene difluoride membrane (Immobilon-P, Millipore) using a Bio-Rad Trans-Blot SD Semi-Dry Transfer Cell device, and blocked in 5% milk in TBST buffer (25 mmol/l Tris pH 7.5, 150 mmol/l NaCl, 0.1% Tween 20) for 1 h at room temperature (RT), then were incubated overnight with antibodies to CD9, CD63, CD81, TSG101, Annexin A5, Integrin β1, integrin α3, filaggrin, transglutaminase2, Lyn, Mhc1 (Santa Cruz Biotechnology), Integrin α2 (Advanced Cellular Biology), and MUC16/CA125 (Dako) at a 1:100 dilution in 5% milk in TBST at 4 °C with gentle rocking. Blots were then washed 3x with TBST for 10 min, and incubated with peroxidase-conjugated goat anti-mouse (#A4416, Sigma-Aldrich) or goat anti-rabbit (#A6667, Sigma-Aldrich) immunoglobulin G secondary antibody, 1:4000 dilution, in 5% milk in TBST for one hour. Blots were washed 3x with TBST for 10 min, developed with SuperSignal West Dura chemiluminescent extended duration substrate kit (ThermoScientific) and visualized with a GE ImageQuant LAS4000 biomolecular imager or a Bio-Rad ChemiDoc MP Imaging System.

In vitro meso-mimetic cell-to-mesothelium adhesion assay

As tumor cell adhesion to peritoneal mesothelial cells is an early event in OvCa metastatic dissemination, an in vitro meso-mimetic assay was used to evaluate the impact of EVs on adhesion of tumor cells to peritoneal mesothelial cells [4, 23]. Human peritoneal mesothelial cells (LP9) were grown for 4 days on 24-well plates previously coated with collagen I resulting in a complete

lawn of live LP9 cells at the bottom of each well on the day of the assay. OvCa cells (human OVCAR5 or murine ID8-Trp53$^{-/-}$) on 6-well plates were grown to 60% confluence, rinsed 3x with PBS and treated with 5×10^7 EVs isolated from young or aged tumor naïve murine peritoneal lavages in 1 ml of the appropriate media for 24 h at 37 °C. For function blocking antibody or inhibitor studies, the EVs were first treated for 3 h with the inhibitor or antibody in 200 µl of media before adding to OvCa cells. The next day, these cells were rinsed 3x with PBS and stained red with CMPTX Cell-Tracker Red or Mito-Tracker Red CMXRos dye (Invitrogen) in serum-free media for 30 min then placed in serum-containing media for 30 min, rinsed with PBS, trypsinized, counted, centrifuged and resuspended at a concentration of 10^4/ml. The 24-well plate containing LP9 cells was washed with PBS and 500 µl of untreated or sEV-treated cells were added to each well. The plate was incubated at 37 °C for 20 min. The cells were then removed and the plate was washed once with PBS. Each well was photographed in 5 fields at 4x magnification on an EVOS or an ECHO microscope. Adherent cells were quantified by Image J. Assays were performed in triplicate in a minimum of triplicate biological replicates. Data were evaluated by Student's *t*-test using Sigmaplot version 15.0 with a *p*-value cutoff of 0.05 defined as statistically significant. Blocking data were analyzed using Kruskal-Wallis test and Dunn's multi-comparison test.

Short-term in vivo adhesion assay

To evaluate the effect of EVs on tumor cell adhesion to mesothelial cells on intact peritoneal tissue, a short-term in vivo adhesion assay was used. RFP-tagged ID8-Trp53$^{-/-}$ murine EOC cells (6×10^6) were treated with EVs from young or aged mice (1.3×10^7) or PBS (controls) for 24 h prior to intra-peritoneal injection into 3–6 month old female mice ($n = 3$/group). After 24 h, mice were euthanized by CO_2 inhalation followed by cervical dislocation. After skin removal, the abdominal cavity was rinsed with PBS and organs were imaged, then dissected and the omentum imaged individually using the IVIS In Vivo Imaging system. Omentum-specific RFP intensity was quantified using Image J as previously described [11, 21, 24]. Data were evaluated by Student's *t*-test using Sigmaplot version 15.0 with a *p*-value cutoff of 0.05 defined as statistically significant.

3-dimensional collagen invasion assay

To evaluate the effect of EV treatment on the ability of OvCa cells to penetrate 3-dimentional collagen gels, an in vitro collagen invasion assay was used. The undersides of 8 µm invasion chambers (Corning #354578 Bedford, MA) in 24-well plates were coated with 500 µl of 100 µg/ml rat tail collagen I diluted in coating buffer (0.1 Na_2CO_3 at pH 9.6) at 37 °C for 2 h. Chambers were rinsed gently with coating buffer. The inside of the chambers was coated with 100 µl of 200 µg/ml collagen I at room temperature and allowed to air dry in the laminar flow tissue culture hood overnight. The inside of the chamber was gently rinsed 3 times with media. OvCa cells which had been untreated or treated with EVs (2×10^8) from young or aged lavages for 24 h at 37 °C were trypsinized, neutralized and collected by centrifugation at 285 g for 2 min. Cells were resuspended at a concentration of 500,000 cells/ml. 200 µl of cells (10^5 cells) was added to the inside of each invasion chamber and placed in a 24-well plate with wells containing 400 µl of media. The plate was incubated for 48 h at 37 °C. A wet Q-tip was used to remove the remaining cells in the inside of each chamber and invaded cells were fixed and stained using the Diff-quick kit (Thermo Fisher Scientific). The filters were excised and mounted using Permount (Fisher Scientific) with the cell side face down, and the entirety of the filter was photographed at 10x power on an Olympus CKX41 microscope and enumerated. Assays were performed in triplicate in a minimum of triplicate biological replicates. Data were evaluated by Student's *t*-test using Sigmaplot version 15.0 with a *p*-value cutoff of 0.05 defined as statistically significant.

sEV proteomics - protein extraction and quantification

Lysis of sEVs was performed using commercial RIPA lysis buffer for the S-Trap digestion method. sEV lysis was promoted by sonication two times for 10 min using an ultrasonic water bath (model no. 97043-988, VWR). Protein samples were precipitated with ice-cold acetone overnight at − 20 °C. Following precipitation, samples were centrifuged at 14,000 g at 4 °C for 30 min, and precipitates were washed with cold acetone, dried, and reconstituted in RIPA lysis buffer. After sEV lysis, protein concentration was determined using the NanoOrange™ Protein Quantitation Kit (Thermo Fisher Scientific) according to the manufacturer's protocol, and samples were aliquoted in 20 µL volumes containing 20 µg of protein.

Protein digestion: suspension trapping (S-Trap) sample preparation

sEV samples denatured and extracted with RIPA buffer were digested through S-Trap following previously described methods [25]. Briefly, proteins were denatured and reduced with 10% SDS and 10 mM TCEP at 95ºC for 10 min with 0.2% DCA included as a passivating agent, and 100 mM TEAB (pH 8) included for buffering. Proteins were alkylated using 10 mM iodoacetamide (IAA) for 30 min at room temperature in the dark. A final concentration of 1.2% of phosphoric acid was used to quench the alkylation reaction. Following manufacturer

instructions, 100 mM TEAB was added to 90% methanol to form a protein suspension which was spun onto an S-Trap device and rinsed. Proteins retained on the S-Trap were digested using sequencing grade Lys-C/trypsin mixture at an enzyme-to-substrate ratio of 1:50 (w/w) in TEAB. Following digestion, peptides were eluted using 100 mM TEAB followed by 0.1% FA in water. The reaction was quenched with 10% FA. A third elution was performed using 50% acetonitrile (ACN) and 0.1% FA. All eluates were combined and dried using a SpeedVac (Fisher Scientific). The resulting peptides were resuspended in 0.1% FA and then desalted and fractionated with poly(styrenedivinylbenzene) reverse phase sulfonate (SDB-RPS) stage tips as described below.

Peptide fractionation

To test whether peptide fractionation is compatible with our sample and could increase the identified number of proteins, we used SDB-RP StageTip following the previously reported method [26]. Briefly, the resulting peptides from each sample preparation method were reconstituted in 0.2% trifluoracetic acid and loaded onto the activated SDB-RP StageTip. Then, peptides were eluted into three consecutive fractions separately, (i) 100 mM ammonium formate, 40% ACN, 0.5% FA, (ii) 150 mM ammonium formate, 60% ACN, 0.5% FA, (iii) 5% ammonium hydroxide, 80% ACN. Each collected fraction was dried using a SpeedVac and reconstituted in 0.1% FA, 4% ACN for mass spectrometry analysis. The proteomic workflow is outlined in Fig. 4A.

Reverse-phase LC-MS/MS analysis

LC – MS/MS analyses were performed using a NanoAQUITY UPLC system (Waters Corporation, Milford, MA), which was coupled online to a Q Exactive™ HF mass spectrometer (Thermo Scientific). Each collected fraction of peptides was reconstituted in 4% ACN and 0.1% formic acid to a concentration of 200 ng/µL and then loaded onto a BEH C18 100 µm × 100 mm column that contained 1.7 µm particles (Waters; Milford, MA). Peptides were separated over a 100 min gradient using a binary solvent system at a flow rate of 0.9 µL/min. The column was heated to 55 °C. Solvent A consisted of water with 0.1% FA while solvent B consisted of ACN with 0.1% FA. The following linear gradient was used for all samples: 4% B for 0–10 min, 4–30% B from 10 to 81 min, 30–88% B from 81 to 85 min, 88% until 88 min, 88–4% B for 1 min, and re-equilibration at 4% B from 89 to 100 min. The mass spectrometer was operated in top 17 data-dependent acquisition mode with automated switching between MS and MS/MS. The ion source was operated in positive ion mode at 1.8 kV, and the ion transfer tube was maintained at 280℃. Full MS scans were acquired from 385 to 1800 m/z at resolution of 60 000, with an AGC target of 3×10^6 ions and a fill time of 80 ms. MS/MS scans were performed from 200 to 2000 m/z at a resolution of 15 000 and a maximum fill time of 100 ms. The AGC target was set at 1×10^5 ions. An isolation window of 2.0 m/z was used for fragmentation with a normalized collision energy of 28. Dynamic exclusion was set at 40 s. Ions with a charge of +1 or greater than +6 were excluded from fragmentation. All samples were run in triplicate.

Proteomic data analysis

All raw LC-MS/MS files were searched using PEAKS proteomics software. The search peptide mass tolerance was set to 10 ppm. Trypsin was set as the digestion enzyme with a maximum of two missed cleavages. Carbamidomethylation was set as a fixed modification, while oxidation (M), acetylation (protein N-term), deamidation (NQ), phosphorylation (HCDR and STY), and ubiquitination were set as variable modifications. For protein identification, MS spectra were searched against the Uniprot *Mus-musculus* (Mouse) protein database downloaded October 2023, and mass error tolerance for precursor and fragment ion was set to 20 ppm and 0.02 DA, respectively. Only proteins with at least two unique peptides were retained for identification (Supplementary File S1). The mass spectrometry proteomics data were deposited to the ProteomeXchange Consortium (http://www.proteomexchange.org) via the PRIDE partner repository with the dataset identifier PXD061884 [27]. Enrichment analyses of Gene Ontology (GO, PANTHER 18.0; https://pantherdb.org) annotations and the Kyoto Encyclopedia of Genes and Genome (KEGG; https://david.ncifcrf.gov) pathways analyses were performed to identify possible enrichment of differentially abundant proteins. Label-free quantification (LFQ) was performed using data dependent analysis (DDA) and the PEAKS package according to default LFQ parameters. The data output from PEAKS was analyzed using OriginPro 2024b, Microsoft Excel and RStudio statistical software.

Results

Isolation and characterization of sEVs

Advanced age is a significant risk factor for OvCa diagnosis in women and aged mice exhibit higher metastatic burden in syngeneic xenograft studies relative to young controls [6–12], suggesting that age-associated changes in the peritoneal microenvironment may impact OvCa progression. sEVs play a major role in intercellular communication, enabling exchange of cargo between source and target cells. To evaluate sEVs present in the peritoneal cavity of healthy mice, peritoneal lavage was performed on young (3–6 month) or aged (20–22 month) mice and sEVs isolated using an asymmetric nanopore membrane isolation technology (NanoEX™, Pleasanton,

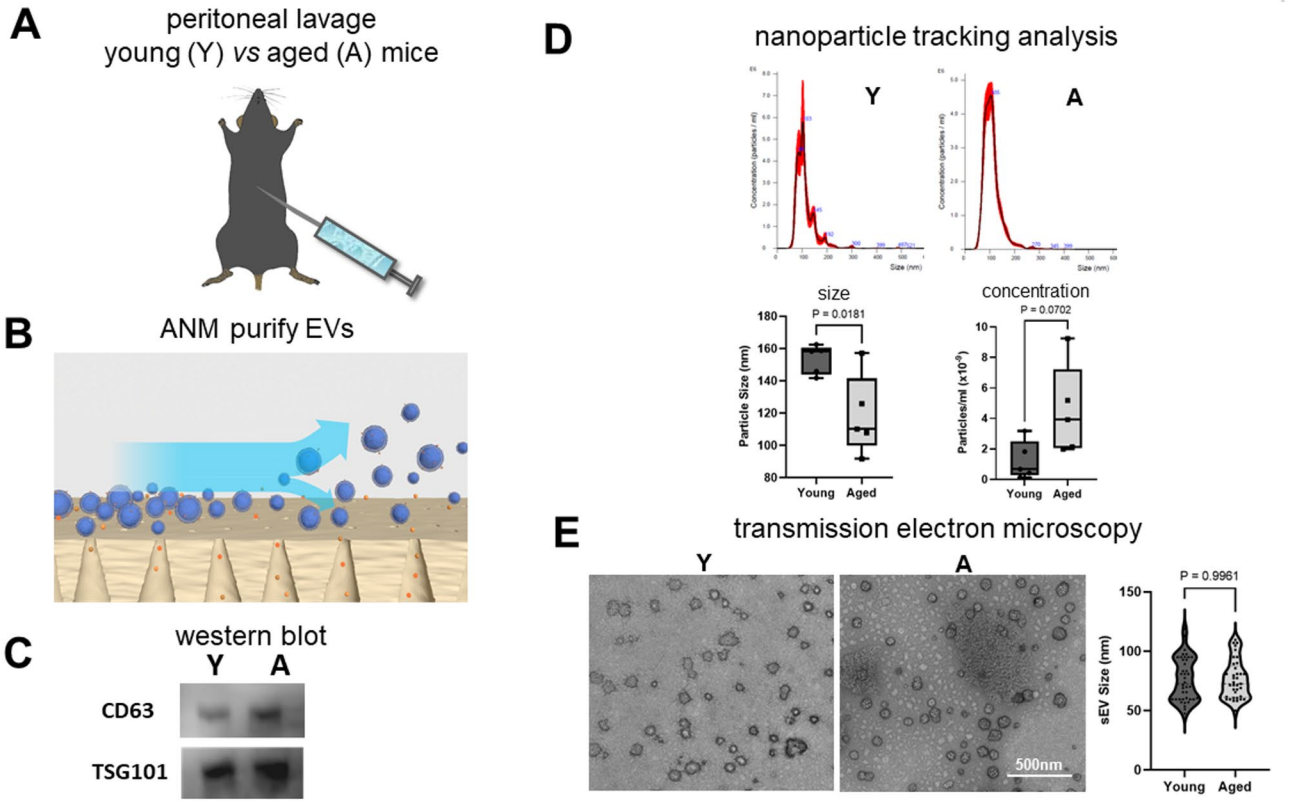

Fig. 1 sEV isolation and characterization. (**A**) Young (3–6 month) and aged (20–22 month) healthy mice ($n = 3$/group) were subjected to peritoneal lavage once a week for 3 weeks. Lavage fluids from each mouse were pooled prior to sEV isolation. (**B**) sEV isolation was accomplished using a NanoEX™ system, a bionanoparticle isolation technology microfluidic cassette housing an asymmetric nanopore membrane, according to the manufacturer's specifications. (**C**) sEVs derived from young and aged peritoneal lavage (20 ug) were electrophoresed on a 9% SDS polyacrylamide gel and western-blotted to PVDF membrane. Blots were probed with antibodies to CD63 and TSG101 at a 1:100 dilution, and with a peroxidase-conjugated rabbit secondary antibody at a 1:4000 dilution. (**D**) NanoSight NS300 nanoparticle tracking analysis was performed immediately following sEV isolation. sEVs typically had a mean size slightly larger than 100 nm with little large particle contaminants. Plots show nanoparticle size and concentration. (**E**) Transmission electron microscopy of sEVs from young and aged mouse lavages. Plot shows nanoparticle size

CA) (Fig. 1A,B). Western blotting demonstrated the presence of the exosome marker proteins CD63 and TSG101 (Fig. 1C) [28]. Characterization by nanoparticle tracking analysis showed a similar EV concentration (Fig. 1D; 1.25×10^9 +/- 0.56×10^9 and 4.50×10^9 +/- 1.32×10^9 particles/ml, $p = 0.07$ for EVs from young and aged lavage, respectively) with mean sizes of 153.5 nm+/-9.05 nm and 118.5 nm+/-24.8 nm ($p = 0.02$) for EVs from young and aged lavage, respectively (Fig. 1D), indicative of small EVs (sEVs). Transmission electron microscopy confirmed the presence of sEVs ranging in size from 51 to 119 nm and 60–110 nm for sEVs from young and aged sEVs, respectively with mean sizes of 76.3 nm+/-18.3 nm and 76.3 nm+/-16.2 nm ($p = 0.99$) for EVs from young and aged lavage, respectively (Fig. 1E).

sEVs from aged host tumor-naïve lavage promote adhesion and invasion of OvCa cells

OvCa exhibits a distinct metastatic mechanism in which cells are exfoliated from the primary tumor into the peritoneal cavity. Shed tumor cells can block peritoneal lymphatics leading to the buildup of ascites fluid that further facilitates metastatic dissemination [3, 4]. Tumor cells adhere to the monolayer of mesothelial cells that lines the peritoneal cavity, whereupon they induce mesothelial cell retraction resulting in exposure of the sub-mesothelial matrix. This matrix is rich in type I collagen, providing a substratum to which OvCa cells avidly adhere and invade to establish widely disseminated metastatic lesions [3, 4]. We have developed an in vitro mesomimetic adhesion assay to mimic early events in OvCa metastatic dissemination that monitors tumor cell adhesion to the human peritoneal mesothelial cell line LP9 grown atop a type I collagen matrix [4, 23]. OvCa cells treated with sEVs from aged peritoneal lavage were significantly more adhesive relative to untreated cells or cells treated with sEVs from young peritoneal lavage (Fig. 2A). Similar results were observed when cells were placed into a Boyden chamber with 3-dimensional collagen gels. OvCa cells treated with sEVs from aged peritoneal lavage

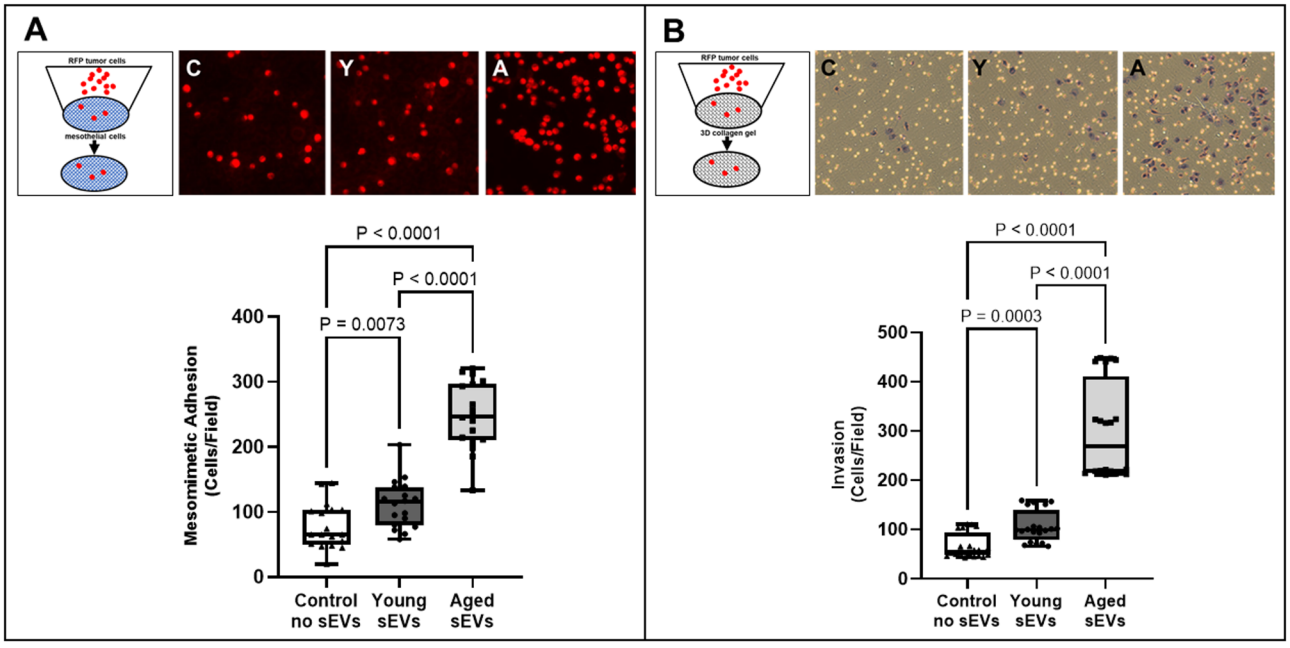

Fig. 2 sEVs from aged host tumor-naïve lavage promote in vitro meso-mimetic adhesion and invasion of human OvCa cells. sEVs (5×10^7) purified from young or aged host peritoneal lavage were added to OVCAR5 cells (5×10^5) and incubated for 24 h. (**A**) Mesomimetic adhesion assay. Upper panel: assay schematic and representative images of adherent cells treated with control (C), young (Y) and aged (A) sEVs. OvCa cells were dyed with Mito-Tracker Red CMXRos dye and cells (5×10^4) were added to a monolayer of LP9 human peritoneal mesothelial cells on type I collagen coated wells 20 min. Non adherent cells were gently rinsed away with PBS and adherent cells were enumerated by counting cells in five 4X fields. (**B**) 3D collagen invasion assay. Upper panel: assay schematic and representative images of invaded cells adherent to the underside of the filter after treatment with control (C), young (Y) and aged (A) sEVs. OvCa cells (5×10^5) were added to a Boyden chamber containing 0.8 µm filter and coated with type I collagen (20 ug). After incubating 48 h, the filter was removed and invaded cells on the bottom of the filter were enumerated by counting cells in five 4X fields. Experiments were performed a minimum of three times and evaluated using student's t-test

exhibited a ~ 3-fold enhancement in collagen invasive activity relative to untreated cells or cells treated with sEVs from young peritoneal lavage (Fig. 2B).

Murine OvCa cells (RFP-tagged ID8-Trp53$^{-/-}$ cells) also exhibited enhanced adhesion in the meso-mimetic assay when treated with sEVs from aged peritoneal lavage relative to both untreated cells and cells treated with sEVs from young peritoneal lavage (Fig. 3A). To examine adhesion in vivo, OvCa cells were pre-treated with sEVs or control buffer prior to i.p. injection. After 24 h, mice were sacrificed, dissected at the midline, and peritoneal organs imaged in situ (Fig. 3B), demonstrating adherent tumor cells on the omentum. The omenta were removed, imaged ex vivo and adherent tumor cells quantified. Results show a significant increase in omental adhesion in vivo of OvCa cells treated with sEVs from aged peritoneal lavage relative to both untreated cells and cells treated with sEVs from young peritoneal lavage (Fig. 3C,D).

Protein identification and comparison of differentially abundant proteins

To identify protein components of sEVs that may contribute to the enhanced adhesive and invasive behavior of OvCa cells, sEV extracts were subjected to LC-MS/MS analysis and PEAKS proteomics software was employed for data analysis [28]. The acquired MS data were used for both protein identification through database searches and quantification by label free quantitation (LFQ) analysis. A total of 5904 and 2437 peptides, as well as 1223 and 509 proteins were identified by database search for aged and young samples, respectively (Fig. 4A). The identified proteins belong to 552 and 245 protein groups, identified by a common set of peptides, for aged and young samples respectively (Fig. 4A). As shown in Fig. 4B, two Venn diagrams illustrate the number of proteins and protein groups identified in the aged and young samples. Out of 1,223 proteins identified in the aged group, 812 are unique to aged, while 411 are in common with the young group. Additionally, out of 526 proteins identified in young, 97 are unique to young. For protein groups, 552 were identified in aged, with 355 being unique to aged and 197 shared with young (Fig. 4B, Suppl. File S1). A volcano plot was generated by plotting $\log_2$ (fold-change, FC) on the x-axis and -$\log_{10}$ (FDR corrected t-test *p* values) on the y-axis (Fig. 4C, Suppl. File S2). Significant differentially abundant proteins were designated with black symbols for upregulated and red symbols for downregulated proteins. In comparison with the young dataset, 854 proteins showed significant changes in the aged dataset

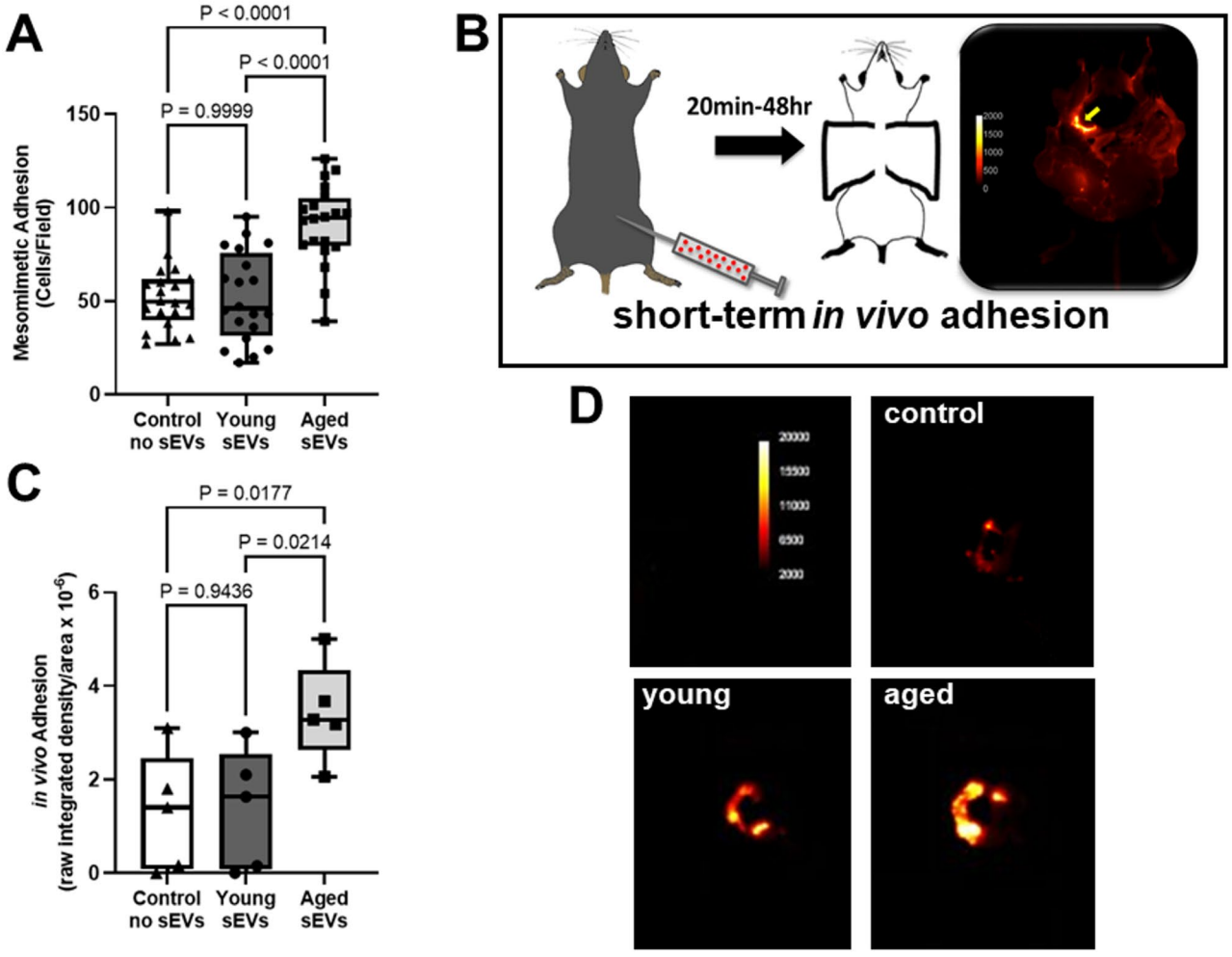

Fig. 3 sEVs from aged host tumor-naïve lavage promote in vitro meso-mimetic and in vivo omental adhesion of murine OvCa cells. sEVs (5×10^7) purified from young or aged host peritoneal lavage were added to RFP-tagged ID8-Trp53$^{-/-}$ (5×10^5) and incubated for 24 h. (**A**) OvCa cells (5×10^4) were then added to a monolayer of LP9 peritoneal mesothelial cells on type I collagen coated wells20 min. Non adherent cells were gently rinsed away with PBS and adherent cells were enumerated by counting cells in five 4X fields. Experiments were performed in triplicate. (**B-D**) To evaluate initial adhesive events in vivo, sEV-treated cells (6×10^6) were injected i.p. into female C57Bl/6 mice. (**B**) After 24 h, a midline dissection was made and the peritoneal cavity imaged in situ. (**C**, **D**) Dissected omenta were imaged ex vivo and RFP fluorescence quantified using ImageJ. Data obtained from $n = 3$ mice/group

including 828 proteins that were up-regulated (FC ≥ 2 and significance ≥ 13) and 26 proteins that were down-regulated (FC < 0.5 and significance ≥ 13).

In order to provide insight into the biological function of differentially expressed proteins in aged and young samples, GO analysis was performed using protein analysis through evolutionary relationships (PANTHER 18.0; https://pantherdb.org) 'molecular function' and 'protein class' tools (Suppl. Files S3 and S4) [29]. The top 'molecular function' categories identified in this analysis for both aged and young groups were 'binding' and 'catalytic activity'. Pie charts depict molecular function (Fig. 5A) and protein classes (Fig. 5B) for both aged and young groups. For GO 'molecular functions' (Fig. 5A), the top categories in both the aged and young groups were 'binding' and 'catalytic activity'. Notably, in the binding group, 46.6% of the proteins in dataset aged and 39.4% in dataset young belong to this category. For 'catalytic activity', 24.8% in dataset aged and 28.1% in dataset young fall into this group. For GO 'protein classes' identified in cohorts aged and young (Fig. 5B), cohort aged includes 21 protein classes while groups young shares 20 protein classes with group aged but lacks RNA metabolism proteins. To categorize further, the distribution of proteins in representative protein classes was compared. There are 86 overlapping binding proteins between cohorts aged and young, while 215 binding-related proteins are uniquely found in cohort aged and 12 are unique to cohort young (Suppl. Figure 1, Suppl. Files 3 and 4). Among these are multiple proteins related to integrin binding, adhesion

A

Name	MS Run	MS1	MS2	PSM	Peptides	Proteins	Protein groups
A	9	105723	243551	28005	5904	1223	552
Y	9	151813	137125	8846	2437	509	245

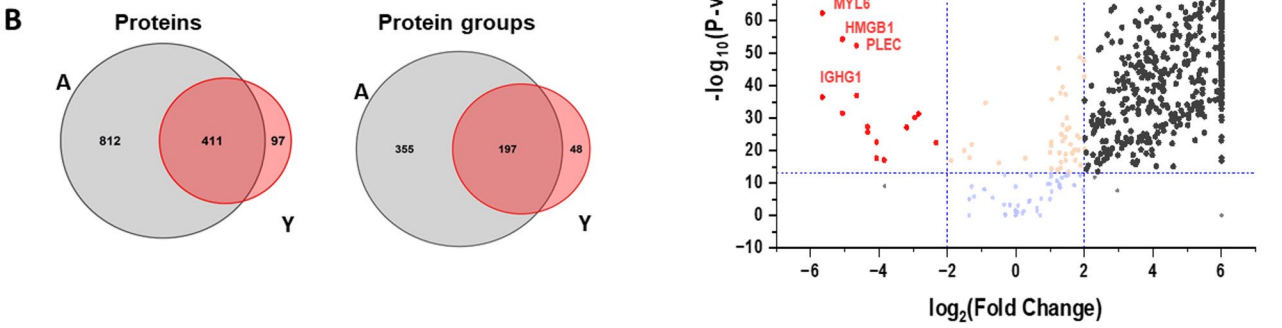

Fig. 4 Proteomic analysis of sEVs isolated from young vs. aged peritoneal lavage. (**A**) Statistical summary of protein identification; the number of MS run, MS1, MS2, PSM, identified peptides, sequences, proteins, and protein groups in aged (A) and young (Y) EVs. (**B**) Venn diagrams display the unique and overlapping protein and protein group identifications across the A and Y groups. (**C**) Volcano plot showing differentially expressed proteins. Black symbols– upregulated proteins; red symbols– downregulated proteins. Selection criteria: up-regulated (FC ≥ 2 and significance ≥ 13) and down-regulated (FC < 0.5 and significance ≥ 13)

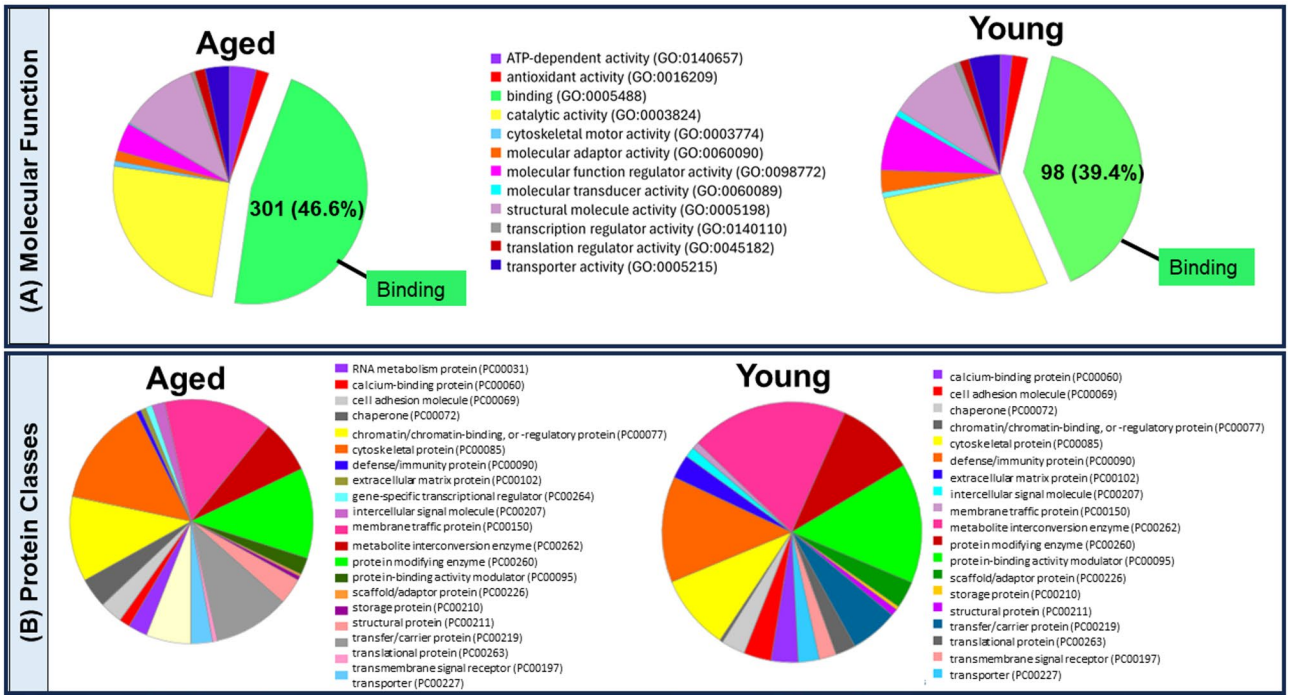

Fig. 5 Comparison of 'molecular function' categories and 'protein classes' in protein datasets obtained from sEVs isolated from young vs aged peritoneal lavage. (**A**) Pie chart of gene ontology 'molecular function' categories in protein datasets from aged and young lavage sEVs. The number of proteins classified as 'binding' is highlighted in each group. (**B**) Pie chart of gene ontology 'protein classes' identified in protein datasets from aged and young lavage sEVs

signaling, and cell motility including VINC, ACTN1 ACTN4, TLN1, TLN2, CAPG, ARP2, SFN, and RAP1B. To gain more insights into the signaling events that might be involved in aging, a pathway analysis was performed using both Panther and DAVID servers. Among the significantly differential proteins identified when comparing the aged and young datasets, PANTHER highlighted the 'integrin signaling' pathway as the top-ranked, with 22

genes. Meanwhile, DAVID identified the top KEGG pathways ($P < 0.05$) as 'regulation of the actin cytoskeleton', 'complement and coagulation cascades', 'focal adhesion', and 'adherens junctions', further emphasizing the critical roles of binding and adhesion in this dataset.

Validation and functional evaluation of selected proteins

Based on the proteomics data and subsequent pathway analyses highlighting integrin binding and cell adhesion, several proteins that were membrane proteins and/or had a known association to ovarian cancer were chosen for validation by western blotting. These include 4 proteins that were found only in sEVs from aged peritoneal lavage (MHC1, LYN, FLG and MUC16/CA125; Suppl. Figure 2A) and additional proteins that were upregulated in aged lavage sEVs relative to young, including CD9, CD63, CD81, ANXA5, TGM1, and ITGB1 (Suppl. Figure 2B). To evaluate whether selected proteins enriched in sEVs from aged peritoneal lavage contribute functionally to the enhanced adhesion observed in OvCa cells treated with aged host sEVs, function blocking antibodies were incubated with sEVs prior to their addition to OvCa cells. Pretreatment of aged sEVs with function blocking antibodies to β1 integrin (ITGB1) (Fig. 6A), mucin 16 (MUC16, CA125) (Fig. 6B) and the Src family tyrosine kinase LYN (Fig. 6C) significantly abrogated the enhanced adhesion induced by aged sEVs, returning adhesion to control levels. Similarly, pretreatment of aged sEVs with the small molecule inhibitor TL0259, that has specificity for the LYN and FGR Src family kinase members (IC_{50} 0.1 nM and 0.03 nM, respectively) also abrogated the aged sEV-induced adhesion of OvCa cells to peritoneal mesothelial cells (Fig. 6D). Statistical analyses for Fig. 6 are in Suppl. Table 1.

Discussion

Aging is a significant risk factor for OvCa incidence and an adverse prognostic factor, with a median overall survival rate of 37.4 months for women over 65 as compared to 47.6 months for women under 65 [5–10]. Among the factors contributing to this survival disparity may be heightened cancer aggressiveness in the aged host. Indeed, recent studies of the peritoneal microenvironment of the aged host have identified senescent omental mesothelial cells and altered omental collagen anisotropy as potential age-related contributors to disease progression [12, 30, 31]. The current study evaluated the role of host-derived sEVs in modulating tumor cell behavior. Results show that sEVs from tumor-naïve aged host peritoneal lavage significantly enhance OvCa tumor cell aggressiveness via modulation of adhesion to peritoneal mesothelial cells and collagen invasion. Proteomic analyses of isolated sEVs identified differential protein cargoes of sEVs from aged host lavage relative to young and function-blocking studies demonstrate a role for several proteins in regulating OvCa cell: mesothelial cell interaction, a key early event in i.p. metastatic dissemination.

Based on the results of the in vitro meso-mimetic binding and in vivo omental adhesion assays, LC-MS/MS proteomics analysis was performed on sEVs to identify protein components that may regulate this fundamental event in i.p. metastasis. Western blotting demonstrates the presence in sEVs of several membrane proteins with known significance in OvCa such as MUC16/CA125, TGM1, MHC1, ITGB1, ITBA2, and ITGA3. Notably, MUC16 (CA125) is a heavily glycosylated mucinous glycoprotein that contributes to heterotypic adhesion to mesothelin present on peritoneal mesothelial cells [32–35]. The shed ectodomain of MUC16 is designated CA125 and is commonly recognized as a biomarker for OvCa recurrence [35–37]. TGM1 is associated with chemoresistance of ovarian cancer cells [38, 39]. MHC1 plays a major role in antigen presentation and elicitation of the immune response. Several studies have reported the presence of MHC1 in sEVs derived from a variety of cell types, suggesting a potential role for sEVs in immune regulation [40–42]. Integrins α2β1 and α3β1 bind sub-mesothelial matrix proteins including type I collagen, facilitating adhesion to and anchoring of OvCa cells within the peritoneal cavity [43, 44]. Pre-incubation of aged sEVs with function-blocking antibodies to either MUC16/CA125 or β1 integrin completely abrogated the sEV-enhanced tumor cell: mesothelial cell adhesion. Similar results were seen with function blocking antibodies to or a small molecule inhibitor of LYN, a non-receptor tyrosine kinase in the SRC family. Although a role for LYN in OvCa has not been described, this kinase regulates neutrophil adhesion by inducing integrin activation [45]. Given that both neutrophils and OvCa cells adhere under conditions of flow, further investigation of LYN in modulation of early events in OvCa metastatic dissemination is warranted. Noteworthy in this regard is previous data from our group identifying a role for the related SRC family kinase FGR, also inhibited by TL0459 with nM affinity, in regulation of OvCa cell adhesion and invasion [46].

Age-related changes in EV content have been reported in both humans and mice [47, 48]. For example, plasma-derived sEVs from aged humans (60–70 y.o., both female and male) contain increased immune-related antigens relative to those from younger individuals (30–40 y.o.) [49]. Several intriguing recent studies have shown that sEVs derived from various compartments of a young host can ameloriate age-related tissue dysfunction. For example, plasma-derived sEVs from young (2 mo.) mice injected i.v. into aged (20 mo.) mice extended lifespan and reversed age-related degenerative changes in multiple tissues by enhancing mitochondrial function [50]. Similarly,

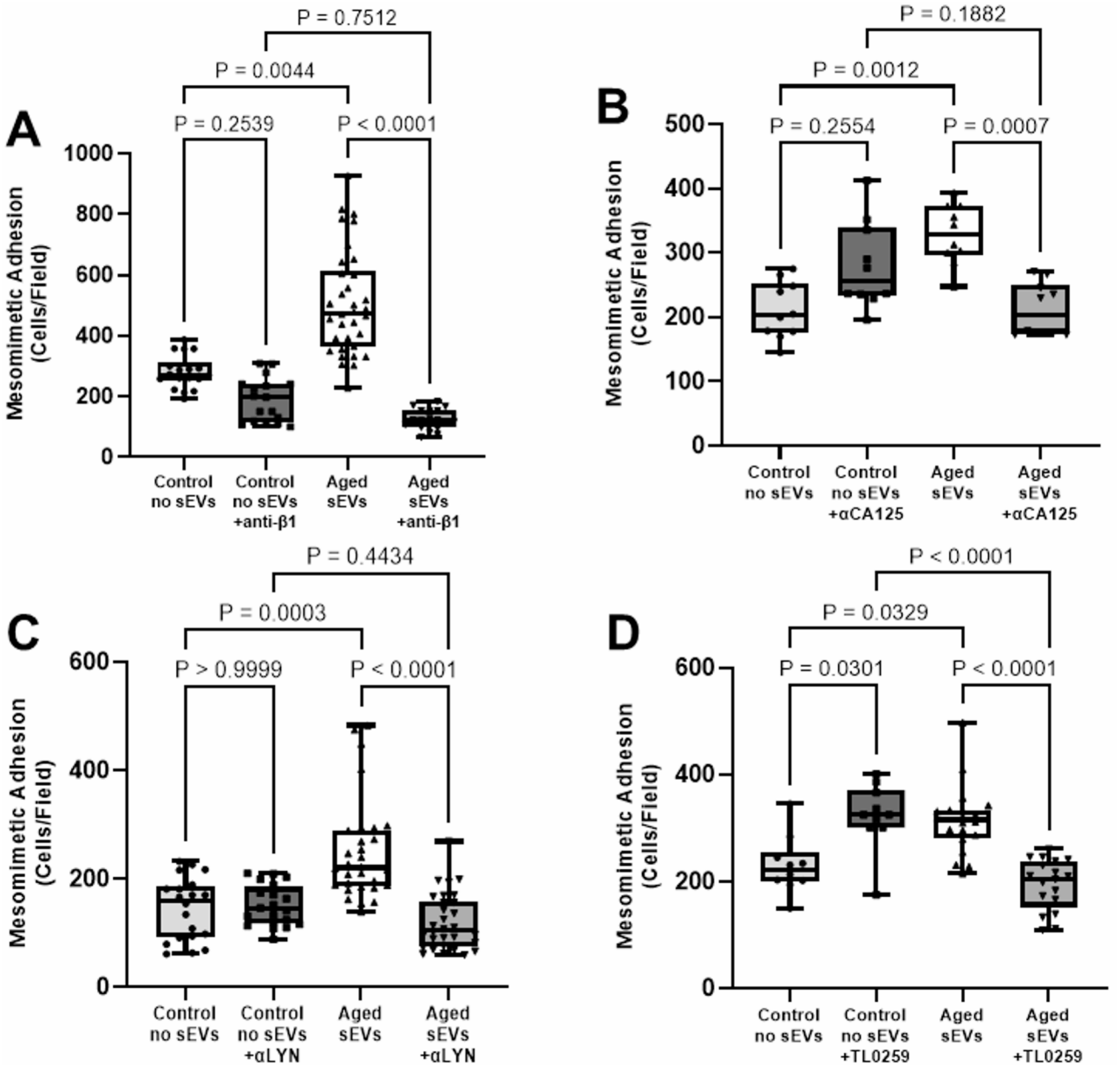

Fig. 6 Blocking sEV-associated proteins abrogates the enhanced meso-mimetic adhesion observed with aged sEVs. sEVs (5×10^7) purified from peritoneal lavage obtained from aged hosts or control (PBS) were incubated with function-blocking antibodies directed against (**A**) β1 integrin (2 μg), (**B**) CA125 (MUC16, 1 μg) or (**C**) LYN kinase (1 μg) in a total volume of 200 ul for 3 h prior to adding to OvCa cells for 24 h. The meso-mimetic adhesion assay was then performed as described in Fig. 3. (**D**) sEVs (5×10^7) purified from peritoneal lavage obtained from aged hosts or control (PBS) were incubated with the Lyn kinase inhibitor TL0259 (0.1 nM) for 3 h prior to adding to OvCa cells for 24 h. The meso-mimetic adhesion assay was then performed as described in Fig. 3. Assays were performed in triplicate. Data were analyzed using Kruskal-Wallis test and Dunn's multi-comparison test

i.p. injection of sEVs isolated from primary fibroblasts obtained from young human donors into aged (22–25 mo.) mice reduced several biomarkers of senescence in multiple tissues and this effect was related to glutathione-S-transferase activity [51]. sEVs obtained from adipose-derived stem cells from young (3–6 mo.) mice injected i.v. into aged (20–24 mo.) mice resulted in reduced frailty, improved physical condition, and a decrease in the estimated epigenetic age of the treated mice [52].

The focus of the current study is on the impact of sEVs derived from the peritoneal lavage fluid of healthy tumor-naïve aged hosts on OvCa tumor cell behavior. Peritoneal sEVs are likely to derive predominantly from the mesothelial monolayer of the peritoneal membrane, a vast serous membrane that lines the inner walls of the abdominal cavity and the outside of the visceral organs with a continuous surface area of 1-2m^2, roughly equivalent to that of the skin [53–56]. Our previous data

demonstrate that sub-mesothelial collagen fibers in aged mice are thicker, more anisotropic and stiffer than those from young mice [12]. Interestingly, recent studies have shown that substratum stiffness alters sEV release and sEV cargo, with cells cultured on a stiffer matrix promoting tumor growth and containing a higher abundance of proteins related to cell adhesion and cell-matrix interactions [57, 58], suggesting a potential mechanism for age-related differences in sEV cargo observed in the current study. However, alterations in the peritoneal immune landscape and enhanced visceral adiposity also accompany aging, such that the contribution of immune cells and adipocytes to the population of sEVs isolated from peritoneal lavage cannot be disregarded.

Conclusion

The tumor microenvironment plays a crucial role in driving both tumor development and metastatic dissemination in OvCa. In addition to sEVs released by healthy host cells and tissues, OvCa tumor cells themselves release sEVs, providing the opportunity for reciprocal sEV-mediated host: tumor communication in the peritoneal *milieu*. OvCa-derived sEVs have been implicated in regulation of adhesion and invasion, stromal remodeling and immune suppression [59–63]. Among the specific functions attributed to sEVs derived from cultured OvCa cells, ascites fluid and patient sera are stimulation of angiogenesis [64, 65], reprogramming of fibroblasts or adipose-derived mesenchymal stem cells to cancer-associated fibroblasts [66, 67], promotion of chemoresistance [60], and alteration of macrophage polarization [68]. Despite this growing understanding, the specific role of sEVs and reciprocal sEV-mediated host-tumor communication in the context of OvCa progression in the aged host is an area in need of further exploration.

Supplementary Information

The online version contains supplementary material available at https://doi.org/10.1186/s12964-025-02273-1.

Supplementary Material 1

Supplementary Material 2

Supplementary Material 3

Supplementary Material 4

Supplementary Material 5

Supplementary Material 6

Supplementary Material 7

Acknowledgements

The authors wish to thank Dr. William Boggess and the University of Notre Dame Mass Spectrometry and Proteomics Facility for expert technical assistance.

Author contributions

Contributions are defined as: (RS) conception and design, data acquisition, analysis and interpretation– mass spectrometry, drafting of manuscript; (JJ) data acquisition, analysis, and interpretation– sEV isolation, western blotting, adhesion and invasion assays; drafting of manuscript; (YL) data acquisition - murine peritoneal lavage; (JY) data acquisition– western blotting, adhesion and invasion assays; (TSH) data acquisition– murine peritoneal lavage, drafting of manuscript; (ZW) data acquisition– sEV isolation; (CB) data acquisition– sEV isolation, adhesion and invasion assays; (JM) data acquisition– sEV isolation, adhesion and invasion assays; (CM) conception and design, data acquisition, interpretation– sEV isolation; (HCC) conception and design– sEV isolation; (RJW) conception and design of work, obtained funding, drafting of manuscript; (MSS) conception and design of work, data analysis and interpretation, drafting and substantial revision of manuscript, obtained funding. All authors read and approved the final manuscript.

Funding

This study was supported in part by Walther Cancer Foundation Cancer Cure Ventures grant (R.S., R.W.), research grants RO1CA109545 and UO1CA236979 from the National Institutes of Health (NIH)/National Cancer Institute (NCI) (M.S.S.), and the Samuel Waxman Cancer Research Foundation (M.S.S.). T.S.H. was supported in part by Research Scientist Development Award KO1CA218305 from the NCI. R.J.W. acknowledges support from the NCI (R21CA267532) and National Institute of General Medical Science (P20GM152280). The NanoExTM was developed in part with support of a Walter Cancer Foundation Cancer Cure Ventures grant (C.W., H.C.C.), by the NIH Commons Fund, through the Office of Strategic Coordination/Office of NIH Director 1UH3CA241684 (H.C.C.) and by research grant R21AI180713 (H.C.C.).

Data availability

The mass spectrometry proteomics data were deposited to the ProteomeXchange Consortium (http://www.proteomexchange.org) via the PRIDE partner repository with the dataset identifier PXD061884.

Declarations

Ethics approval and consent to participate

Studies involving mice were carried out with the approval of the University of Notre Dame Animal Care and Use Committee.

Consent for publication

Not applicable.

Competing interests

The authors declare no competing interests.

Author details

[1]Department of Chemistry and Biochemistry, Seton Hall University, South Orange Village, NJ, USA
[2]Department of Chemistry & Biochemistry, University of Notre Dame, Notre Dame, IN, USA
[3]Harper Cancer Research Institute, University of Notre Dame, A200 Harper Hall, 1234 N. Notre Dame Ave., South Bend, Notre Dame, IN 46617, USA
[4]Department of Biology, Tuskegee University, Tuskegee, AL, USA
[5]Department of Chemical and Biomolecular Engineering, University of Notre Dame, Notre Dame, IN, USA
[6]Aopia Biosciences, Pleasanton, CA, USA
[7]Department of Chemistry, University of Kansas, Lawrence, KS, USA

Received: 7 April 2025 / Accepted: 27 May 2025
Published online: 01 July 2025

References

1. Huang J, Chang WC, Ngai CH, Lok V, Zhang L, Lucero-Prisno DE, et al. Worldwide burden, risk factors, and temporal trends of ovarian cancer: a global study. Cancers. 2022;14. https://doi.org/10.3390/cancers14092230
2. Howlader N et al., SEER Cancer Statistics Review, 1975–2014. Natl Cancer Inst. vol. Bethesda, MD, Apr. 2017. https://seer.cancer.gov/csr/1975_2014/

3. Lengyel E. Ovarian cancer development and metastasis. Am J Path. 2010;177:1053–64.
4. Lengyel, et al. Epithelial ovarian cancer experimental models. Oncogene. 2014;33:3619–33.
5. Yancik R. Ovarian cancer: age contrasts in incidence, histology, disease stage at diagnosis, and mortality. Cancer. 1993;71:517–23.
6. Thigpen T, Brady MA, Omura GA, Creasman WT, McGuire WP, Hoskins WJ, et al. Age as a prognostic factor in ovarian carcinoma. Gynecologic Oncol Group Experience Cancer. 1993;71:606–14.
7. Tew WP, Lichtman SM. Ovarian cancer in older women. Semin Oncol. 2008;35:582–9.
8. Hightower RD, Nguyen HN, Averette HE, Hoskins W, Harrison T, Steren A. National survey of ovarian carcinoma. IV: patterns of care and related survival for older patients. Cancer. 1994;73:377–83.
9. Deng F, Xu X, Lv M, Ren B, Wang Y, Guo W, et al. Age is associated with prognosis in serous ovarian carcinoma. J Ovarian Res. 2017;10:36. https://doi.org/10.1186/s13048-017-0331-6
10. Trillsch F, Woelber L, Eulenburg C, Braicu I, Lambrechts S, Chekerov R, et al. Treatment reality in elderly patients with advanced ovarian cancer: a prospective analysis of the OVCAD consortium. J Ovarian Res. 2013;6:42. https://doi.org/10.1186/1757-2215-6-42
11. Loughran EA, Leonard AK, Phan RC, Stack MS, et al. Aging increases susceptibility to ovarian cancer metastasis in murine allograft models and alters B cell composition in peritoneal adipose tissue. Neoplasia. 2018;20:621–31.
12. Harper EI, Hilliard TS, Sheedy EF, Carey P, Wilkinson P, Siroky MD, et al. Another wrinkle with age: aged collagen and intra-peritoneal metastasis of ovarian cancer. Aging Cancer. 2022;3(2):116–29. https://doi.org/10.1002/aac2.12049
13. Pascual-Antón. et.al. Mesothelial-to-mesenchymal transition and exosomes in peritoneal metastasis of ovarian cancer. Int J Mol Sci. 2021;22(21):11496. https://doi.org/10.3390/ijms222111496. PMID: 34768926.
14. Abbasi-Malati. Tumorigenic and tumoricidal properties of exosomes in cancers; a forward look. Cell Commun Signal. 2024;22(1):130. https://doi.org/10.1186/s12964-024-01510-3
15. Gurunathan. A comprehensive review on factors influences biogenesis, functions, therapeutic and clinical implications of exosomes. Int J Nanomed. 2021;16:1281–312.
16. Mashouri. Exosomes: composition, biogenesis, and mechanisms in cancer metastasis and drug resistance. Mol Cancer. 2019;18:75. https://doi.org/10.1186/s12943-019-0991-5
17. Lin. Extracellular vesicle-cell adhesion molecules in tumours: biofunctions and clinical applications. Cell Commun Signal. 2023;21:246. https://doi.org/10.1186/s12964-023-01236-8
18. Kok VC, Yu CC. Cancer-derived exosomes: their role in cancer biology and biomarker development. Int J Nanomed. 2020;15:8019–36.
19. Paskeh. Emerging role of exosomes in cancer progression and tumor microenvironment remodeling. J Hematol Oncol. 2022;15:83. https://doi.org/10.1186/s13045-022-01305-4
20. Walton J, et al. CRISPR/Cas9-mediated Trp53 and Brca2 knockout to generate improved murine models of ovarian high-grade serous carcinoma. Cancer Res. 2016;76:6118–29.
21. Liu Y, Metzinger MN, Lewellen KA, Cripps SN, Carey KD, Harper EI, et al. Obesity contributes to ovarian cancer metastatic success through increased lipogenesis, enhanced vascularity, and decreased infiltration of M1 macrophages. Cancer Res. 2015. https://doi.org/10.1158/0008-5472.can-15-0706
22. Flurkey K et al. Chapter 20 - Mouse models in aging research. In: Fox JG, Davisson MT, Quimby FW, Barthold SW, Newcomer CE, Smith AL, editors. The Mouse in Biomedical Research (Second Edition), Academic Press, Burlington. 2007:637–672.
23. Kenny, et al. Organotypic models of metastasis: a three-dimensional culture mimicking the human peritoneum and omentum for the study of the early steps of ovarian cancer metastasis. Cancer Treat Res. 2009;149:335–51.
24. Lewellen KA, et al. Quantitation of intra-peritoneal ovarian cancer metastasis. J Vis Exp. 2016. https://doi.org/10.3791/53316
25. Zougman A, Selby PJ, Banks RE. Suspension trapping (STrap) sample preparation method for bottom-up proteomics analysis. Proteomics. 2014;14:1006–1000.
26. Rappsilber J, Mann M, Ishihama Y. Protocol for micro-purification, enrichment, pre-fractionation and storage of peptides for proteomics using stagetips. Nat Protoc. 2007;2:1896–906.
27. Deutsch EW, Bandeira N, Perez-Riverol Y, Sharma V, Carver J, Mendoza L, et al. The proteomexchange consortium at 10 years: 2023 update. Nucleic Acids Res. 2023;51:D1539–48.
28. Welsh JA, Goberdhan DCI, O'Driscoll L, Buzas EI, Blenkiron C, Bussolati B, et al. Minimal information for studies of extracellular vesicles (MISEV2023): from basics to advanced approaches. J Extracell Vesicles. 2024;13:e12404.
29. Thomas PD, Campbell MJ, Kejariwal A, Mi H, Karlak B, Daverman R, et al. PANTHER: a library of protein families and subfamilies indexed by function. Genome Res. 2003;13:2129–41.
30. Książek K, et al. Senescent peritoneal mesothelial cells promote ovarian cancer cell adhesion: the role of oxidative stress-induced fibronectin. Am J Pathol. 2009;174:1230–40.
31. Ksiazek K. Mesothelial cell: a multifaceted model of aging. Ageing Res Rev. 2013;12:595–604.
32. Bruney L, et al. Membrane-type I matrix metalloproteinase-dependent ectodomain shedding of mucin16/ CA-125 on ovarian cancer cells modulates adhesion and invasion of peritoneal mesothelium. Biol Chem. 2014;395:1221–31.
33. Rump A, et al. Binding of ovarian cancer antigen CA125/MUC16 to mesothelin mediates cell adhesion. J Biol Chem. 2004;279:9190–8.
34. Gubbels JA. Mesothelin-MUC16 binding is a high affinity, N-glycan dependent interaction that facilitates peritoneal metastasis of ovarian tumors. Mol Cancer. 2006;5:50. https://doi.org/10.1186/1476-4598-5-50
35. Scholler N, et al. Development of a CA125-mesothelin cell adhesion assay as a screening tool for biologics discovery. Cancer Lett. 2007;247:130–6.
36. Bast RC, et al. A radioimmunoassay using a monoclonal antibody to monitor the course of epithelial ovarian cancer. N Engl J Med. 1983;309:883–7.
37. Moore RG, et al. Current state of biomarker development for clinical application in epithelial ovarian cancer. Gynecol Oncol. 2010;116:240–5.
38. Ding Y, et al. Molecular characteristics and tumorigenicity of ascites-derived tumor cells: mitochondrial oxidative phosphorylation as a novel therapy target in ovarian cancer. Mol Oncol. 2021;15:3578–95.
39. Chan CY, et al. Identification of potential protein targets in extracellular vesicles isolated from chemotherapy-treated ovarian cancer cells. Curr Issues Mol Biol. 2023;45:7417–31.
40. Harshman SW, et al. Proteomic characterization of circulating extracellular vesicles identifies novel serum myeloma associated markers. J Proteom. 2016;136:89–98.
41. Neyrinck-Leglantier D, et al. Immunoregulatory molecule expression on extracellular microvesicles in people living with HIV. Front Immunol. 2024;15:1354065.
42. Synowsky SA, et al. The major histocompatibility complex class I immunopeptidome of extracellular vesicles. J Biol Chem. 2017;292:17084–92.
43. Moser TL, et al. Evidence for preferential adhesion of ovarian epithelial carcinoma cells to type I collagen mediated by the alpha2beta1 integrin. Int J Cancer. 1996;67:695–701.
44. Ellerbroek SM, et al. Ovarian carcinoma regulation of matrix metalloproteinase-2 and membrane type 1 matrix metalloproteinase through beta1 integrin. Cancer Res. 1999;59:1635–41.
45. He Y, et al. The non-receptor tyrosine kinase Lyn controls neutrophil adhesion by recruiting the CrkL-C3G complex and activating Rap1 at the leading edge. J Cell Sci. 2011;124:2153–64.
46. Asem M, et al. Host Wnt5a potentiates microenvironmental regulation of ovarian cancer metastasis. Cancer Res. 2020;80:1156–70.
47. Manni G, et al. Extracellular vesicles in aging: an emerging hallmark?? Cells. 2023;12:527. https://doi.org/10.3390/cells12040527
48. Robbins PD. Extracellular vesicles and aging. Stem Cell Invest. 2017;4:98. https://doi.org/10.21037/sci.2017.12.03
49. Prattichizzo F, Micolucci L, Olivieri F, et al. Exosome-based immunomodulation during aging: a nano-perspective on inflamm-aging. Mech Ageing Dev. 2017;168:44–53.
50. Chen X, et al. Small extracellular vesicles from young plasma reverse age-related functional declines by improving mitochondrial energy metabolism. Nat Aging. 2024;4:814–38.
51. Fafian-Labora JA, et al. Small extracellular vesicles have GST activity and ameliorate senescence-related tissue damage. Cell Metab. 2020;32:71–86.
52. Sanz-Ros J, et al. Small extracellular vesicles from young adipose-derived stem cells prevent frailty, improve health span, and decrease epigenetic age in old mice. Sci Adv. 2022;8:eabq2226. https://doi.org/10.1126/sciadv.abq2226
53. Sodek KL, Murphy KJ, Brown TJ, Ringuette MJ. Cell-cell and cell-matrix dynamics in intraperitoneal cancer metastasis. Cancer Metastasis Rev. 2012;31:397–414.
54. Young VJ, Brown JK, Saunders PT, Horne AW. The role of the peritoneum in the pathogenesis of endometriosis. Hum Reprod Update. 2013;19:558–69.

55. Yung S, Chan T-M. Peritoneal mesothelial cells and the extracellular matrix. Nephrology. 2001;6:250–8.
56. Witz CA, Montoya-Rodriguez IA, Cho S, Centonze VE, Bonewald LF, Schenken RS. Composition of the extracellular matrix of the peritoneum. J Soc Gynecol Investig. 2001;8:299–304.
57. Sneider A, et al. Small extracellular vesicles promote stiffness-mediated metastasis. Cancer Res Commun. 2024;4:1240–52.
58. Wu B, Liu D-A, Guan L, Myint PK, Chin L, Dang H, et al. Stiff matrix induces exosome secrfetion to promote tumour growth. Nat Cell Biol. 2023;25:415–24.
59. Graves LE, et al. Proinvasive properties of ovarian cancer ascites-derived membrane vesicles. Cancer Res. 2004;64:7045–9.
60. Feng W, et al. Exosomes promote pre-metastatic niche formation in ovarian cancer. Mol Cancer. 2019;18:124. https://doi.org/10.1186/s12943-019-1049-4
61. Tian W, et al. Extracellular vesicles in ovarian cancer chemoresistance, metastasis, and immune evasion. Cell Death Dis. 2022;13:64. https://doi.org/10.1038/s41419-022-04510-8
62. Gong L, et al. Tumor-derived small extracellular vesicles facilitate omental metastasis of ovarian cancer by triggering activation of mesenchymal stem cells. Cell Commun Signa. 2024;22:47. https://doi.org/10.1186/s12964-023-01413-9
63. Shen J, et al. Advances of exosome in the development of ovarian cancer and its diagnostic and therapeutic prospect. Onco Targets Ther. 2018;11:2831–41.
64. Yi H, et al. High grade ovarian cancer secreting effective exosomes in tumor angiogenesis.comparative study. Int J Clin Exp Pathol. 2015;8:5062–70.
65. Millmaggi D, et al. Tumor vesicle-associated CD147 modulates the angiogenic capability of endothelial cells. Neoplasia. 2007;9:349–57.
66. Giusti I, et al. Ovarian cancer-derived extracellular vesicles affect normal human fibroblast behavior. Cancer Biol Ther. 2018;19:722–34.
67. Cho JA, et al. Exosomes from ovarian cancer cells induce adipose tissue-derived mesenchymal stem cells to acquire the physical and functional characteristics of tumor-supporting myofibroblasts. Gynecol Oncol. 2011;123:379–86.
68. Chen X, et al. Exosomes derived from hypoxic epithelial ovarian cancer can deliver MicroRNAs to macrophages and elicit a tumor-promoted phenotype. Cancer Lett. 2018;435:80–91.

Publisher's note